Check for updates

Received: 4 July 2024 | Accepted: 7 January 2025

DOI: 10.1002/vzj2.20397

Vadose Zone Journal

ORIGINAL ARTICLE

Special Section: The Contribution of the 8th Galileo Conference to Innovative Ground- and Remote-Based Sensing Approaches to Critical Zone Research

A simple experiment to trace stemflow infiltration: Advantages and challenges of using stable isotopes of hydrogen and oxygen and electrical resistivity tomography

G. Zuecco[1,2] | C. Marchina[1] | M. Censini[3] | D. Todini-Zicavo[1,4] | G. Cassiani[3] | M. Borga[1]

[1]Department of Land, Environment, Agriculture and Forestry, University of Padova, Legnaro, Italy

[2]Department of Chemical Sciences, University of Padova, Padova, Italy

[3]Department of Geosciences, University of Padova, Padova, Italy

[4]University School for Advanced Studies (IUSS), Pavia, Italy

Correspondence
G. Zuecco, Department of Land, Environment, Agriculture and Forestry, University of Padova, Legnaro, Italy.
Email: giulia.zuecco@unipd.it

Assigned to Associate Editor Nunzio Romano.

Funding information
Ministero dell'Istruzione, dell'Università e della Ricerca, Grant/Award Number: PRIN 2017 code: 2017SL7ABC

Abstract

Stemflow is a key process in forested catchments due to its control on soil water content and nutrients' transport. However, there are still few studies focusing on stemflow infiltration and relying on direct observations that are minimally invasive and repeatable. In this study, we exploited the usefulness of stable isotopes of hydrogen and oxygen, as well as of time-lapse electrical resistivity tomography (ERT) to investigate water fluxes in the soil. Specifically, we aimed to examine the effectiveness of both isotopes and ERT to trace stemflow infiltration for a beech tree in a steep hillslope in the Italian pre-Alps, to quantify stemflow infiltration area based on the two methodologies and to provide recommendations for future research. Results showed that both approaches identified an infiltration along the maximum slope gradient with most of the water staying in the upper 45 cm of soil. The analysis of electrical resistivity variations enabled to evaluate the temporal dynamics of stemflow infiltration and to estimate an average stemflow infiltration area of 0.64 m^2, which was larger than values found by previous studies based on dye tracers. This high estimate may be due to multiple factors, from the soil conditions to methodological uncertainties. Conversely, the estimation of stemflow infiltration area based on isotopes was affected by the sampling area. Hence, future research based on isotopic tracers needs to consider methods providing a direct field evidence of stemflow infiltration (e.g., dye tracers) or a quick inspection of raw data (e.g., ERT) to inform the sampling design.

Plain Language Summary

This study explores stemflow, the process of rainwater flowing down tree trunks, which is important for soil water and nutrient distribution in forests. Two methods were used to investigate how stemflow water moves through soil: stable isotopes of

Abbreviations: BEST, Beerkan Estimation of Soil Transfer parameters; ERT, electrical resistivity tomography; GPR, ground penetrating radar; LMWL, Local Meteoric Water Line; RMS, root mean square.

This is an open access article under the terms of the Creative Commons Attribution License, which permits use, distribution and reproduction in any medium, provided the original work is properly cited.
© 2025 The Author(s). *Vadose Zone Journal* published by Wiley Periodicals LLC on behalf of Soil Science Society of America.

hydrogen and oxygen, and time-lapse electrical resistivity tomography (ERT). The study focused on a beech tree on a steep hillslope in the Italian pre-Alps. Both methods showed that stemflow mainly infiltrated along the steepest part of the site and stayed in the top 45 cm of soil. ERT allowed to observe how stemflow infiltration changed over time and to estimate an affected area of 0.64 m^2, larger than values found in previous studies. The effectiveness of the isotopic method depended on soil sample locations. Results suggest that future studies using isotopes should combine them with methods that provide direct visual evidence of water movement (like dye tracers) or quick data checks (like ERT) to improve sampling strategies.

1 | INTRODUCTION

In forested ecosystems, vegetation plays a central role in controlling the transport, the distribution, and the uptake of water and nutrients in the soil. Canopies and stems affect rain water distribution by three processes, namely interception, throughfall, and stemflow. While throughfall is the fraction of rain water that passes through canopies (it can or cannot have a contact with the vegetation) and falls or drips to the ground, stemflow comprises rain water that is channeled by branches and stems and reaches the ground very close to the stem base. Several studies have shown how throughfall and stemflow influence the spatial and temporal patterns of soil water content (e.g., Bialkowski & Buttle, 2015; Bouten et al., 1992; Metzger et al., 2017; Molina et al., 2019) and nutrients (e.g., Guerrieri et al., 2015; Levia & Frost, 2006; Oyarzún et al., 2004; Zimmermann et al., 2008). Despite the vast literature on ecohydrological processes, the investigation of water fluxes under forest canopies remains challenging and requires interdisciplinary perspectives to better understand the role of different processes on catchment water balance and nutrient cycling and the drivers of water infiltration in the soil (e.g., Orlowski et al., 2023; Van Stan & Pinos, 2024).

Compared to other processes taking place in forested catchments, stemflow generally receives less attention, likely due to the underestimated volumes reported in previous research (Germer et al., 2010), and the assumption that stemflow constitutes a small component of the catchment water balance, despite the large fluxes measured at the tree scale (mean stemflow input per tree varying between 0.09 and 7.69 L/h in the previous studies considered for Table 2 in Carlyle-Moses et al. [2018]). Hence, there are still various challenges and open research questions related to the investigation of stemflow. In a recent perspective paper, Van Stan and Pinos (2024) examined three fundamental questions regarding stemflow and which require further research and answers. These questions are "whence stemflow?" (i.e., the origin of stemflow or how tree architecture and which branches contribute to this process), "how much stemflow?" (i.e., the full range of physical conditions determining stemflow, which include not only rain, but also the quantification of stemflow generating from dew, ice, and snowmelt), and "whither stemflow?" (i.e., the fate of this process, which is related to its infiltration at the base of the plants). Regarding the last question, recent papers have raised a discussion about the approaches that have been or could be used to trace stemflow infiltration and quantify its area (e.g., Carlyle-Moses et al., 2020; Llorens et al., 2022; Van Stan & Allen, 2020). Indeed, accurate and direct observations about the spatial extension of stemflow infiltration, how quickly stemflow enters the soil under different conditions and how the wetting front expands in different directions can provide useful insights on the double-funneling effect (i.e., the flow of water along stem, tree roots, and macropores) and the infiltration capacity of forested soils. For instance, Liang et al. (2011) applied dye tracers on a steep hillslope and found that stemflow was mainly concentrated at the downslope side of the tree (species: *Stewartia monadelpha*), and it was diverted by vertical and horizontal roots reaching deeper soil layers as bypass flow. On the contrary, Gonzalez-Ollauri et al. (2020) observed that stemflow of sycamore trees infiltrated as matrix flow and was correlated with the vertical distribution of the roots.

Direct observations of stemflow infiltration are rare (Carlyle-Moses et al., 2020; Van Stan & Allen, 2020), and therefore, such area is usually estimated based on the ratio between stemflow input rate and the mean soil infiltration capacity (e.g., Herwitz, 1986; E. R. C. Reynolds & Henderson, 1967). Among the methodological approaches that we can find for a direct observation of stemflow infiltration, there is the application of dye tracers. Previous studies have proven the usefulness of dye tracers for testing the double-funneling hypothesis (Gonzalez-Ollauri et al., 2020; Pinos et al., 2023; Schwärzel et al., 2012; Spencer & van Meerveld, 2016) and for estimating stemflow infiltration area (Llorens et al., 2022; Pinos et al., 2023). Estimations of stemflow infiltration area vary across study sites and trees and depend on experiment characteristics (i.e., antecedent soil moisture, stemflow intensity and amount) with values between 0.0035 and 0.0951 m^2

15391663, 2025, 1, Downloaded from https://acsess.onlinelibrary.wiley.com/doi/10.1002/vzj2.20397 by University Of Padova Center Di, Wiley Online Library on [07/02/2025]. See the Terms and Conditions (https://onlinelibrary.wiley.com/terms-and-conditions) on Wiley Online Library for rules of use; OA articles are governed by the applicable Creative Commons License

in Llorens et al. (2022), of 0.14 m^2 in Pinos et al. (2023) and up to 0.245 m^2 in Schwärzel et al. (2012). However, experiments based on dye tracers require large excavation, and therefore, are destructive and non-repeatable on the same soil profile (Orlowski et al., 2023).

Recently, Metzger et al. (2021) used soil physical and chemical properties to investigate stemflow, whereas Van Stan and Allen (2020) proposed experiments based on stable isotopes of hydrogen (^2H) and oxygen (^{18}O) as a possible alternative to dye tracers. The application of isotopically labeled water could provide an unambiguous signal that allows the quantification of the fraction of new stemflow in soil water mixtures (Van Stan & Allen, 2020). Indeed, designing artificial experiments using stemflow with an isotopic composition significantly different from that of soil water has the following potential advantages: (1) enabling a clear identification of the stemflow in the soil at different depths and distances, (2) allowing for the application of simple mixing models to quantify the proportion of stemflow in the soil water mixture, (3) permitting the estimation of the residence time of such stemflow in the soil, and (4) enabling to further trace the uptake of stemflow by the plants. Furthermore, stable isotopes of hydrogen and oxygen serve as conservative tracers (i.e., the isotopic composition of water changes only through mixing and evaporation), and they are not affected by the sorption effect typical of the dye tracers. However, similarly to dye tracers, an isotopically labeled approach can be quite destructive because it requires soil sampling at different depths and distances from the tree trunk, to determine the stemflow infiltration area and volume. Recently, Pinos et al. (2023) performed a stemflow experiment on Scots pine by using a dual-labelling approach (enriched ^2H and brilliant blue FCF). They found the prevalence of preferential flow in the soil and a good correlation between δ^2H and brilliant blue FCF concentrations, which diminished with the increasing distance from the tree trunk. Despite the promising results obtained by the dual-labelling approach used by Pinos et al. (2023), there are still no studies relying on stable isotopes of hydrogen and oxygen to investigate stemflow infiltration.

Alternative approaches to destructive methods are represented by measurements of soil water content (Llorens et al., 2022; Pinos et al., 2023) and geophysical methods (Brighenti et al., 2024; Cassiani et al., 2016; Preti et al., 2018). Indeed, soil water content and geophysical surveys are much less invasive and involve considerably less excavations (only for the installations of probes and electrodes) compared to methods based on dye and isotopic tracers. Recent applications of geophysical methods, such as electrical resistivity tomography (ERT), showed successful observations of the temporal dynamics and the spatial patterns of the soil water content and stemflow infiltration (e.g., Cassiani et al., 2015; Dick et al., 2018; Guo et al., 2020; Mary et al., 2018). For instance, Zuo et al. (2021) integrated a dye experiment with ERT measurements to show the role of roots of *Achnatherum splendens* on infiltration processes and soil water distribution. Their findings provided evidence of the relations between root traits and changes in the soil water content using both ERT and the dye tracer. Similarly, Di Prima et al. (2022) combined time-lapse ground penetrating radar (GPR) surveys and different infiltration tests. Their results showed the links between non-uniform flow and different types of soil heterogeneity, and they found evidence of the preferential flow generated along coarse roots during the stemflow infiltration experiment. Another advantage of ERT and GPR surveys is the possibility of obtaining 2D and 3D representations of the subsurface to trace the wetting front, with an approach that is minimally invasive and repeatable compared to destructive methods.

Compared to dye experiments combined with geophysics, there are still no studies that rely on both the use of geophysical methods and stable isotopes of hydrogen and oxygen for the investigation of stemflow infiltration. In this view, there is the need to compare the results of isotope-based experiments with time-lapse geophysical surveys taken at different times before, during, and after the tracer application. Furthermore, new studies should test both methods for the estimation of the stemflow infiltration area and provide recommendations for their application with the aim of designing experiments that are repeatable and less invasive. A clear identification of the infiltration area (and volume) should be possible if an experiment relies on isotopically labeled water with a composition very different compared to that of pre-experiment soil water, and it is possible to identify marked changes in electrical resistivity in the subsurface before and after the tracer application. Significant changes in the electrical resistivity compared to the pre-experiment survey can be detected or enhanced if salt is mixed with the water used for the experiment, particularly when there is poor contact between the electrodes and the soil or the ground material (e.g., Pavoni et al., 2023). Therefore, in this study, we present a simple experiment carried out in a forested catchment in the Italian pre-Alps to simulate stemflow by using isotopically labeled water mixed with salt,

Core Ideas

- Stable isotopes of hydrogen and oxygen and time-lapse ERT were successfully applied to study stemflow infiltration.
- Estimates of stemflow infiltration area were larger than those found in the literature.
- Experiments based on time-lapse ERT are more effective and less invasive than those based on isotopic tracers.

15391663, 2025, 1, Downloaded from https://acsess.onlinelibrary.wiley.com/doi/10.1002/vzj2.20397 by University Of Padova Center Di, Wiley Online Library on [07/02/2025]. See the Terms and Conditions (https://onlinelibrary.wiley.com/terms-and-conditions) on Wiley Online Library for rules of use; OA articles are governed by the applicable Creative Commons License

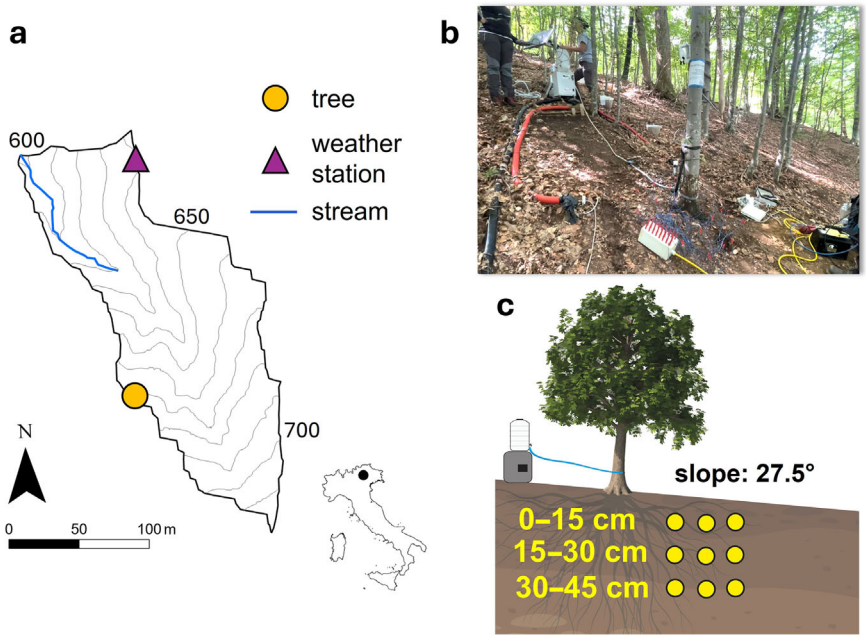

FIGURE 1 Ressi experimental catchment and its geographical location in Italy (a), picture of the setup taken during the stemflow experiment (b), and sketch of the setup and the sampling depths for soil (c).

and to trace the stemflow signature in the soil. The specific objectives of this study are to:

1. verify the usefulness of stable isotopes of hydrogen and oxygen to trace stemflow infiltration,
2. analyze time-lapse electrical resistivity data to investigate the temporal dynamics of the expansion of the wetting front,
3. compare estimates of stemflow infiltration area based on electrical resistivity variation data, isotopic data, and the classical indirect method derived from the ratio between stemflow input rate and the mean soil infiltration capacity,
4. provide recommendations for future applications of stemflow experiments based on isotopic tracers and electrical resistivity data.

2 | MATERIALS AND METHODS

2.1 | Study area

The stemflow experiment was carried out at a beech tree (*Fagus sylvatica* L.) located in Ressi experimental catchment, a small, forested catchment located in the Italian pre-Alps (Zuecco et al., 2021; Figure 1a). Catchment elevations range from 598 to 721 m a.s.l., and the climate is humid temperate. In the period 2012–2022, the average air temperature was 10.1°C, whereas the average annual precipitation was 2115 mm. The bedrock consists of rhyolites and dacites. Soil is classified as Cambisol and generally, the topsoil (0–10 cm) has a sandy clay loam texture, whereas deeper in the profile, the soil has a sandy clay texture (Penna et al., 2015; Zuecco et al., 2021). Soil bulk density is 1.18 g/cm^3, indicating a loose soil, and the porosity is about 55% (average of three soil samples in the upper 20 cm). The catchment is covered by a dense forest, dominated by beech, chestnut, maple, and hazel trees (Penna et al., 2015; Zuecco et al., 2021). The beech tree chosen for the experiment is located on a hillslope in the upper part of Ressi catchment, where the average slope is 27.5° (Figure 1b,c). The beech tree has a 12.4-cm diameter and a stem area of 0.02 m^2 at its base, and it was chosen for the experiment because it was already investigated by geophysics (this setup is shown in Figures 1b and 2). The stem lean measured at the ground level by a hand-held inclinometer is 8°; such value indicates the likely occurrence of preferential flow of stemflow (Pinos et al., 2021).

2.2 | Set up of the stemflow experiment

The experiment was conducted on September 6–7, 2022, after a week without rainfall events during a particularly dry year (Xia et al., 2024), to better trace the labeled water signature in a soil with a low water content (Figure S1). In the period September 1–6, 2022, the precipitation amount recorded at the weather station located outside the forest (Figure 1a) was only 0.4 mm. During the stemflow experiment, 1 mm of rain fell on September 7 between 3:00 a.m. and 10:20 a.m. but had no influence on the soil water content measured at three sites located about 1 m away from the beech tree (Figure S1). Hence, we consider that this small rainfall amount had a negligible effect on our findings. At the very beginning of the experiment, one sensor recorded a slight increase in the soil water content (Figure S1), which was related to the first ERT measurement when some labeled water was applied to the downslope boreholes (see Section 2.4 for details).

15391663, 2025, 1, Downloaded from https://acsess.onlinelibrary.wiley.com/doi/10.1002/vzj2.20397 by University Of Padova Center Di, Wiley Online Library on [07/02/2025]. See the Terms and Conditions (https://onlinelibrary.wiley.com/terms-and-conditions) on Wiley Online Library for rules of use; OA articles are governed by the applicable Creative Commons License

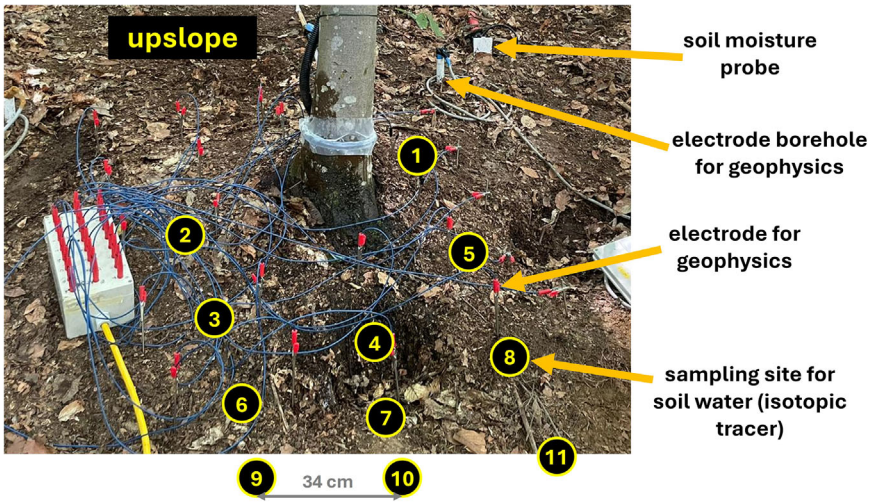

FIGURE 2 Setup for the geophysical surveys and location of the sites used for soil samplings. Location 1 is slightly upslope of the tree, whereas locations 9, 10, and 11 are few centimeters downslope of the picture. The electrodes for the geophysical surveys were 20 cm spaced.

We simulated stemflow with a rate equal to 6.6 L/h for a total volume of 26 L. Our stemflow intensity was similar to Pinos et al. (2023) (7 L/h), but much lower compared to Llorens et al. (2022) (range of 31–290 L/h). The experiment setup followed the procedure of Llorens et al. (2022). A PVC flexible plastic tube was used to simulate stemflow (Figure 1b,c). The tube was drilled with 2-mm holes (every 4 cm), it was installed around the beech tree about 20 cm above the ground, and it was connected to a tank with a valve to regulate the water flux. The tank was placed ~1.5 m above the ground, upslope of the tree, to take advantage of the elevation gradient to let the water flow to the tree trunk. The water flow from the container was regulated by two valves.

For the stemflow experiment, we applied labeled water with an isotopic composition (expressed using the δ notation) very different compared to the isotopic composition of soil water during the summer months; δ^2H of labeled water was −88.8‰ and δ^{18}O was −12.92‰, whereas three soil samples collected at 10-, 30-, and 60-cm depth at a nearby hillslope location were considered pre-experiment soil water (δ^2H was −29.6 [average] ±3.0 [standard deviation] ‰ and δ^{18}O was −3.51±1.00‰). Furthermore, salt (NaCl) was added to the labeled water (and therefore, used as a second tracer) to increase the electrical conductivity (which was 1072 µS/cm) of stemflow infiltrating into the soil and favor resistivity measurements with ERT. The simulated stemflow lasted almost 4 h, but the whole experiment that included geophysical surveys and soil sampling for isotopic analysis lasted more than 24 h. The experiment ended in the afternoon of September 7, 2022, after the collection of the soil samples.

2.3 | Soil sampling, soil water extraction, and isotopic analyses

Soil sample collection for isotopic analysis was carried out about 24 h after the end of the stemflow simulation, at three depths (0–15, 15–30, and 30–45 cm; Figure 1c) and at 11 locations close to the tree trunk (Figure 2). Locations were selected between the electrodes for ERT (less-disturbed soil) and avoiding surficial roots. Location 1 was chosen for its slightly upslope position. Thirty-two soil samples were collected by a manual auger with a 5-cm diameter. The soil was quickly homogenized, small stones and root pieces were removed, and then an aliquot of the sample was put in a 12-mL glass Exetainer vial (Labco Ltd.). Afterward, samples were stored in a fridge at 4°C until the soil water extraction.

Soil water was extracted using the cryogenic vacuum distillation method based on Koeniger et al. (2011) at the Free University of Bozen-Bolzano (Italy). The description of the extraction method and setup can be found in Amin et al. (2021) and Zuecco et al. (2022). Soil water samples were then analyzed for isotopic composition by off-axis cavity output spectroscopy (DLT-100 analyzer, Los Gatos Research Inc.) at the Department of Land, Environment, Agriculture and Forestry of the University of Padova (Italy), following the procedure described in Marchina et al. (2020). All water samples were calibrated with standards relative to the Vienna Standard Mean Ocean Water.

2.4 | Geophysical surveys

A 3D ERT-based investigation was performed using a system of 72 electrodes. Among these, 48 electrodes were divided into modules of 12 electrodes each, spaced 10 cm from each other, and housed in four boreholes with a diameter of ~5 cm (Figure 2). These boreholes were positioned at the vertices of a square with 120-cm sides, each reaching a depth of 120 cm. This arrangement placed the 48 electrodes along the edges of the cubic volume under study. The remaining 24 electrodes were arranged on the surface around the tree, forming the vertices of a 20-cm squared mesh grid (Figure 2).

15391663, 2025, 1, Downloaded from https://acsess.onlinelibrary.wiley.com/doi/10.1002/vzj2.20397 by University Of Padova Center Di, Wiley Online Library on [07/02/2025]. See the Terms and Conditions (https://onlinelibrary.wiley.com/terms-and-conditions) on Wiley Online Library for rules of use; OA articles are governed by the applicable Creative Commons License

TABLE 1 Time schedule of the electrical resistivity tomography (ERT) surveys and indication of the start and end of the stemflow simulation.

Date and time	Time from start of the injection (h:min)—it corresponds to the average time of the ERT acquisition	ERT dataset	Comment
06/09/2022 11:30	–	t0	Start of the background ERT measurement
06/09/2022 12:50	00:00	–	Start of the stemflow simulation
06/09/2022 13:05	00:15	t1	
06/09/2022 14:05	01:15	t2	
06/09/2022 15:30	02:40	t3	
06/09/2022 16:35	03:45	t4	
06/09/2022 16:45	03:55	–	End of the stemflow simulation
06/09/2022 17:30	04:40	t5	
06/09/2022 18:45	05:55	t6	
07/09/2022 09:25	20:35	t7	
07/09/2022 11:50	23:00	t8	

The installation of the system for the ERT measurements was completed several months prior to the stemflow experiment. Due to the poor soil cohesion in the study area, resulting from the loose soil and a high state of alteration (due to the drilling of the boreholes), we hypothesized that the manually augered electrode boreholes experienced lateral displacement over time. This likely reduced the contact between some of the electrodes and the surrounding soil. Such an issue created difficulties during the current-sending phases of data acquisition, leading to increased noise in the data and anomalously high resistivity values that may not accurately represent the electrical properties of the soil. To mitigate this issue and enhance the signal of interest, for the stemflow experiment, we increased the electrical conductivity of the water to 1072 µS/cm, which is well above the average electrical conductivity of soil water (167 µS/cm, $n = 216$) collected in the lower part of Ressi catchment (Zuecco et al., 2021). This adjustment enabled us to capture the dynamics of the wetting front despite the aforementioned technical challenges. Furthermore, during the background ERT measurement (t0, Table 1), to improve the contact between the electrodes and the surrounding soil, we had to add about 100 mL of labeled water in the downslope boreholes to favor the circulation of electric current.

During the experiment, nine geophysical measurements (from t0 to t8, Table 1) were acquired using a Syscal Pro Switch 72ch (IRIS Instruments). The acquisition sequence followed a Dipole-Dipole skip 4 scheme, with the recording of both direct and reciprocal measurements of the apparent electrical resistivity. Complete reciprocal acquisition, exchanging the potential with the current electrodes, was performed to estimate acquisition errors and eliminate anomalous elements before data inversion (Binley & Kemna, 2005). This ERT data acquisition is defined as "ERT time-lapse technique" and can be combined to controlled irrigation experiments (Cassiani et al., 2009). Table 1 reports the time schedule of the stemflow experiment with indication of the acquired ERT datasets.

2.5 | Data analysis

2.5.1 | Analysis of isotopic data and estimation of the fraction of labeled water

δ^2H and δ^{18}O of soil water were compared visually to the isotopic composition of pre-experiment soil water and labeled water by using a dual-isotope plot, where we added the Local Meteoric Water Line (LMWL) of Ressi catchment built based on isotopic data of rain water collected in the period 2019–2022. The dual-isotope plot was also used to identify possibly marked deviations of soil water samples from the LMWL due to evaporation or bad injections during the isotopic analysis.

To estimate the fraction of labeled water at each location and depth for soil sampling, we applied a two-component mixing model based on δ^{18}O (Pinder & Jones, 1969; Sklash & Farvolden, 1979). We assumed that soil water was a mixture of pre-experiment soil water and labeled water used for the stemflow simulation. Equations at the basis of the two-component mixing model were as follows:

$$psw + lw = 1, \tag{1}$$

$$\delta_{sw} = psw \times \delta_{psw} + lw \times \delta_{lw}, \tag{2}$$

15391663, 2025, 1, Downloaded from https://acsess.onlinelibrary.wiley.com/doi/10.1002/vzj2.20397 by University Of Padova Center Di, Wiley Online Library on [07/02/2025]. See the Terms and Conditions (https://onlinelibrary.wiley.com/terms-and-conditions) on Wiley Online Library for rules of use; OA articles are governed by the applicable Creative Commons License

where *psw*, *lw*, and *sw* indicate the pre-experiment soil water, the labeled water, and the considered soil water sample, respectively, and the notation δ represents $\delta^{18}O$.

Then, Equations (1) and (2) were solved for the unknown *lw* (expressed as percentage), as follows:

$$lw = \frac{\delta_{sw} - \delta_{psw}}{\delta_{lw} - \delta_{psw}} \times 100. \quad (3)$$

The uncertainty in the estimated fraction of labeled water was calculated according to the error propagation method at the 5% confidence level (Genereux, 1998). This approach accounts for the instrumental precision during the isotopic analysis (0.25‰ was considered for $\delta^{18}O$), the statistical significance in relation to the number of pre-experiment soil water samples ($n = 3$), and the difference in $\delta^{18}O$ of pre-experiment soil water and labeled water (9.41‰). The fraction of labeled water and its uncertainty were estimated for all 32 sites for soil sampling, and the uncertainty varied between 0.8% and 4.6%, with an average of 3.3%.

Computations and plots based on isotopic data were performed using MATLAB R2024a (MathWorks), Microsoft Excel, and PowerPoint (Microsoft Corporation).

2.5.2 | Analysis of electrical resistivity

The processing of the ERT datasets was conducted using ResIPy (Blanchy et al., 2020). This software facilitates importing, filtering, and error modeling of geoelectrical data and employs the mature R2 and R3t inversion codes developed by Binley and Kemna (2005) for solving direct current resistivity problems. R2 and R3t are finite element-based codes that allow for the incorporation of complex topography and the modeling of bounded regions. They offer full flexibility in electrode assignment, accommodating both surface and borehole electrode-based surveys. The inverse modeling in these codes uses a weighted least squares objective function coupled with a range of regularization options, including time-lapse data analysis (Binley, 2015).

Data were initially imported and filtered using ResIPy, considering a 10% error threshold between direct and reciprocal measurements. This allowed us to discard potentially erroneous measurements that may have arisen from the previously noted in-hole electrode contact issues. This error threshold was selected based on the site conditions, characterized by poor soil cohesion and a high presence of air in the first meter of the subsurface, which is not favorable for the circulation of electric current. This 10% error level was also considered as the intrinsic error level of the data and was set as a target for the root mean square (RMS) value in the inversion and regularization process. This aimed to yield a reliable resistivity distribution model within the explored volume. The use of a highly conductive salt solution to simulate stemflow improved the system's ability to circulate electric current, particularly within the volume affected by the wetting front, thus enhancing the information density.

During the inversion phase, we used a background constrained inversion approach. This method penalizes subsequent surveys for deviations from the reference survey, enabling the observation of variations in electrical resistivity between datasets relative to the initial background measurement (t0). In this study, to highlight the differences between the ERT surveys, we plotted and analyzed for each survey (from t1 to t8) the resistivity variations (expressed in percentage) with respect to the t0 inverted model. Given the application of some labeled water in the downslope boreholes (during t0) to favor the circulation of the electric current, we discarded the volume of soil corresponding to the boreholes before the analysis of the electrical resistivity data.

Electrical resistivity (in a logarithmic scale) and their variations compared to t0 were displayed in ParaView 5.12.0 (Kitware Inc.). Electrical resistivity variations were used to determine frequencies of mesh elements in each class of resistivity variation; classes had a step of 10% from −100% to 0%, whereas we grouped together in one class variations ≥0%. The positive variations observed during the inversion phase can be attributed to the model's effort to minimize the misfit between calculated and measured data. As the stemflow infiltration advances, there is a progressive increase in the volume affected by a reduction in electrical resistivity. From a regularization perspective, the presence of a region with decreasing resistivity relative to the initial background condition compels the software to generate artificial resistivity increases (artifacts) in the model. These artifacts are an inevitable consequence of abrupt changes in conductivity between the wet and the dry domains and do not impact the overall value of the obtained results.

2.5.3 | Estimation of the stemflow infiltration area

Stemflow infiltration area was estimated using three different approaches. The first method is applied when there are no direct observations of stemflow infiltration (Llorens et al., 2022). In this study, we used the approach proposed by Carlyle-Moses et al. (2018), which assumes that during the stemflow experiment, the soil surface has reached saturation and a constant infiltration rate. Based on this assumption, I_t (i.e., stemflow infiltration area based on this indirect method) was estimated as follows:

$$I_t = \frac{S_{r_t}}{K_{sat}}, \quad (4)$$

15391663, 2025, 1, Downloaded from https://acsess.onlinelibrary.wiley.com/doi/10.1002/vzj2.20397 by University Of Padova Center Di, Wiley Online Library on [07/02/2025]. See the Terms and Conditions (https://onlinelibrary.wiley.com/terms-and-conditions) on Wiley Online Library for rules of use; OA articles are governed by the applicable Creative Commons License

where S_{r_t} represents the stemflow input rate (6.6 L/h) and K_{sat} is the saturated hydraulic conductivity at the soil surface. K_{sat} was determined by a simplified approach developed by Bagarello et al. (2013, 2014), who compared it to the BEST (Beerkan Estimation of Soil Transfer parameters) procedure. Therefore, in March 2023, to estimate K_{sat}, we performed simple infiltration tests at eight locations close to the beech tree (3–10 m away from the trunk). For these tests, we used a 7.5-cm radius (r) metallic ring, inserted to a depth of about 1–2 cm into the soil surface to avoid lateral loss of the ponded water (Bagarello et al., 2014). K_{sat} was then computed for all eight locations as follows:

$$K_{sat} = \frac{b_1}{0.467 \times \left(\frac{2.92}{r \times \alpha*} + 1\right)}, \quad (5)$$

where b_1 is the slope of the linearized cumulative infiltration curve and $\alpha*$ is the parameter describing the relative importance of gravity and capillary flow for ponded infiltration (Bagarello et al., 2014). Here, we used a value of 0.012 mm^{-1} for $\alpha*$ because it is considered the value of first approximation for most field soils (W. D. Reynolds et al., 2002). The average K_{sat} was 422 mm/h, whereas the standard deviation was 418 mm/h. The cumulative infiltration curve was determined by relating $\frac{If}{\sqrt{t_{If}}}$ and $\sqrt{t_{If}}$, where If is the cumulative infiltration and t_{If} is the cumulative times needed for water to infiltrate into the soil. Based on these eight K_{sat} values, we determined eight values for I_t.

The second approach we used for estimating stemflow infiltration area was based on electrical resistivity variations. From t1 vs. t0 to t8 vs. t0, we determined the surface area (upper 2 cm of the mesh) with resistivity variations values $<-10\%$ (values varying between 0 and -10% were considered uncertain due to artifacts). These surface areas were considered equivalent to the stemflow infiltration areas, and the eight obtained values were used for comparison with the results of the first and the last approach.

As third approach, we decided to spatially interpolate the fraction of labeled water estimated at the 0–15 cm depth (the shallowest sampling layer). During the preparation of the input data for the spatial interpolation, we used a conservative approach and accounted for the uncertainty in the estimation of the fraction of labeled water, that is, at each location, we used the difference between the estimated fraction and its uncertainty value (in case of negative differences, we set them equal to 0%). For the spatial interpolation, we applied the inverse distance weighting technique in ArcGIS Pro 3.3.0 (Esri Inc.). We varied the maximum and the minimum number of locations used for the interpolation, as well as the semiaxis value and the sector type, and we optimized the power. Then, we retained the two spatial interpolations which yielded the best results in terms of cross-validation, that is, a leave-one-out resampling method used to evaluate spatial interpolation models (the lowest root mean square error [RMSE] was 16.8%). Afterward, we reclassified the interpolated rasters by considering three classes of fraction of labeled water, that is, equal to 0%, comprised between 0% and 5% and >5%. We decided to use three classes because we observed a higher uncertainty in the interpolation for values of fraction of labeled water >0% and ≤5%. Based on this reclassification, we computed two stemflow infiltration areas, corresponding to a fraction of labeled water >0% and to a fraction >5%. We note here that limitations of this approach are due to the small number of sampling sites and the lower surface area covered with the soil sampling compared to the electrical resistivity variation data. However, this spatially interpolated area was used for comparison with the other approaches to examine the limitations of our study and provide recommendations for future stemflow experiments.

3 | RESULTS

3.1 | Isotopic variations in soil water

At the end of the stemflow experiment, soil water samples had an isotopic composition intermediate between the signatures of (the more enriched) pre-experiment soil water and of (the more depleted) labeled water (Figure 3). Pre-experiment soil water had an isotopic composition intermediate between two bulk rain water samples collected in the period August 11–September 6. Most of the soil water samples plotted to the right side of the LMWL, in agreement with the slight evaporative signature of pre-experiment soil water. Soil water collected at 0–15 cm was the least affected by the input of labeled water (four samples plotted very close or within the error bars of pre-experiment soil water), whereas samples at 15–30 cm were the most affected by labeled water (Figure 3).

The sampling locations of soil water showing the most depleted isotopic composition were the closest to the tree trunk, downslope and along the maximum slope gradient (Figure 4a), which corresponded to locations 4 and 7 in Figure 2. These very depleted values are also consistent with the field observation of some overland flow generating at the stem base and moving downslope toward location 4. The spatial variability in the isotopic composition of soil water indicated that the lateral distribution of the infiltrated stemflow did not affect the upper right corner of the sampling volume (Figure 4a). Results of the two-component mixing model showed that the fraction of labeled water varied between $-7.6\pm4.6\%$ (this implies that there was no isotopic variation at this location during the experiment) and $82.5\pm0.8\%$, with an average of $23.9\pm3.3\%$ (Figure 4b). The average fraction of labeled water was $18.7\pm3.5\%$ ($n = 11$), $28.8\pm3.1\%$ ($n = 11$), and $24.3\pm3.3\%$ ($n = 10$) at the 0–15 cm,

15391663, 2025, 1, Downloaded from https://acsess.onlinelibrary.wiley.com/doi/10.1002/vzj2.20397 by University Of Padova Center Di, Wiley Online Library on [07/02/2025]. See the Terms and Conditions (https://onlinelibrary.wiley.com/terms-and-conditions) on Wiley Online Library for rules of use; OA articles are governed by the applicable Creative Commons License

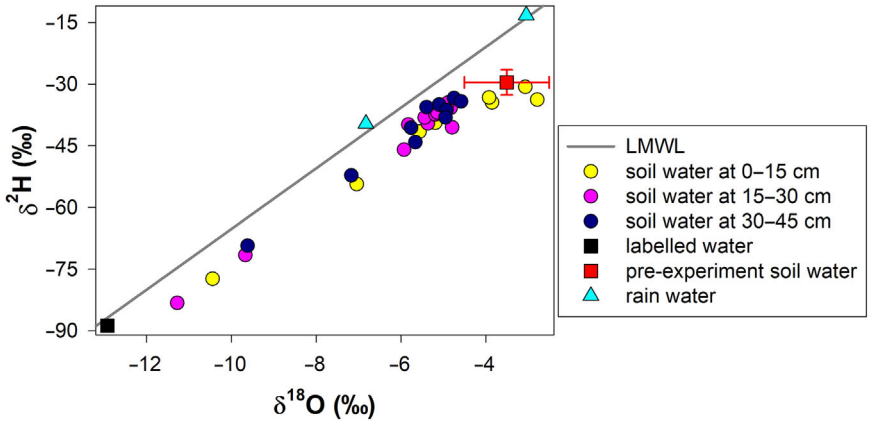

FIGURE 3 Dual-isotope plot for soil water collected at 0–15 cm, 15–30 cm, and 30–45 cm depths; labeled water; and pre-experiment soil water. Error bars represent standard deviation of three samples of pre-experiment soil water collected at 10-, 30-, and 60-cm depth at a nearby hillslope location. Local Meteoric Water Line (LMWL) of Ressi catchment is plotted in gray, and it refers to the 2019–2022 period ($\delta^2H = 7.38 \times \delta^{18}O + 8.56$). Two bulk rain water samples collected in the period August 11, 2022–September 6, 2022, are also shown.

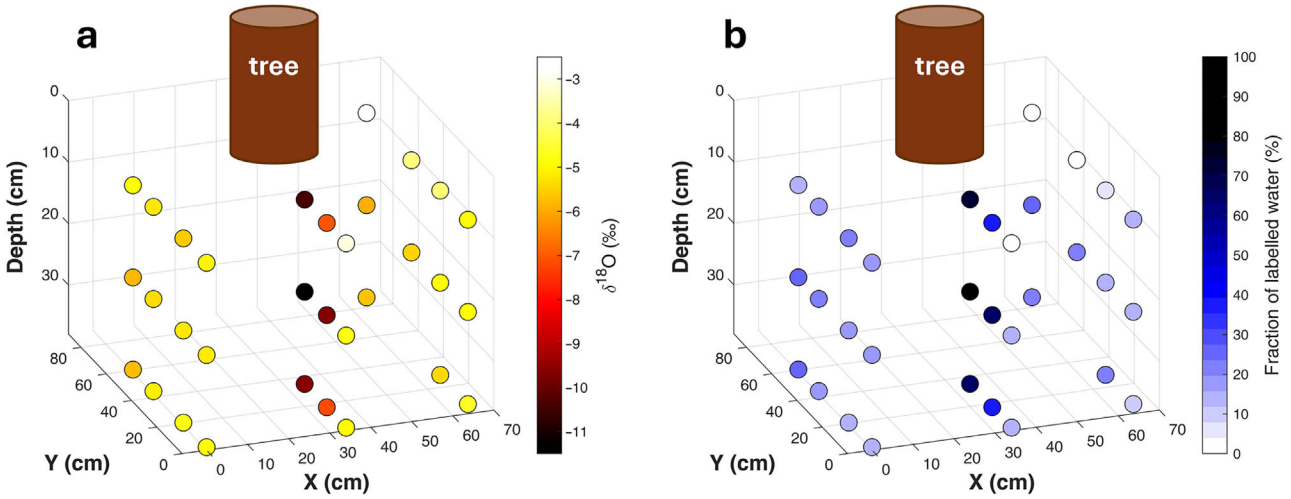

FIGURE 4 $\delta^{18}O$ values of soil water (a) and fraction of labeled water determined at three depths and at different locations (b). For a better view of the samples, circles were drawn at the average depths, that is, 7.5 cm (for 0–15 cm), 22.5 cm (for 15–30 cm), and 37.5 cm (for 30–45 cm).

15–30 cm, and 30–45 cm depths, respectively. The estimated fraction of labeled water suggests that there was a clear replenishment by stemflow, except at four locations (white/light blue dots in the upper layer, Figure 4b) corresponding to locations 1, 5, and 10 in Figure 2.

3.2 | Electrical resistivity variations

Electrical resistivity values were generally high (>1000 Ωm) before, during, and at the end of the stemflow experiment (Figure 5). For t0, we observed that resistivity was slightly lower on the surface ground (values varying between 10 and 800 Ωm) close to the tree trunk, and at depths >80 cm (particularly upslope) probably due to the presence of a more conductive soil layer. From t1 to t8, we observed less resistive values only on the surface ground and at shallow depths due to the infiltration of the labeled water with high electrical conductivity (Figure 5). Indeed, negative differences (i.e., below −20%) in resistivity were observed only on a small portion of the investigated soil volume (Figure 6). As expected, electrical resistivity variations were more marked toward the end of the experiment (t6 vs. t0 and t8 vs. t0, Figure 6) than at the beginning (t1 vs. t0 and t3 vs. t0, Figure 6), due to the expansion of the wetting front. These differences in electrical resistivity for different surveys showed that most of the labeled water moved downslope, but it generally remained in the upper 40–50 cm (Figure 6). Furthermore, the most negative resistivity variations were found close to the location where the largest fraction of labeled water was estimated based on the isotopic tracer (Figure 4b).

The computation of the frequency of mesh elements grouped based on resistivity variation classes confirmed that during the experiment, there were no significant changes (i.e., resistivity variations were equal to zero or even positive) in more than 35% of the mesh elements (Figure 7a). Most of negative variations were between 0% and −30%, and overall, the shapes of the frequency distributions were quite similar, except for t1 vs. t0, t2 vs. t0 (the infiltration was ongoing, and the wetting front still had to reach its maximum

15391663, 2025, 1, Downloaded from https://acsess.onlinelibrary.wiley.com/doi/10.1002/vzj2.20397 by University Of Padova Center Di, Wiley Online Library on [07/02/2025]. See the Terms and Conditions (https://onlinelibrary.wiley.com/terms-and-conditions) on Wiley Online Library for rules of use; OA articles are governed by the applicable Creative Commons License

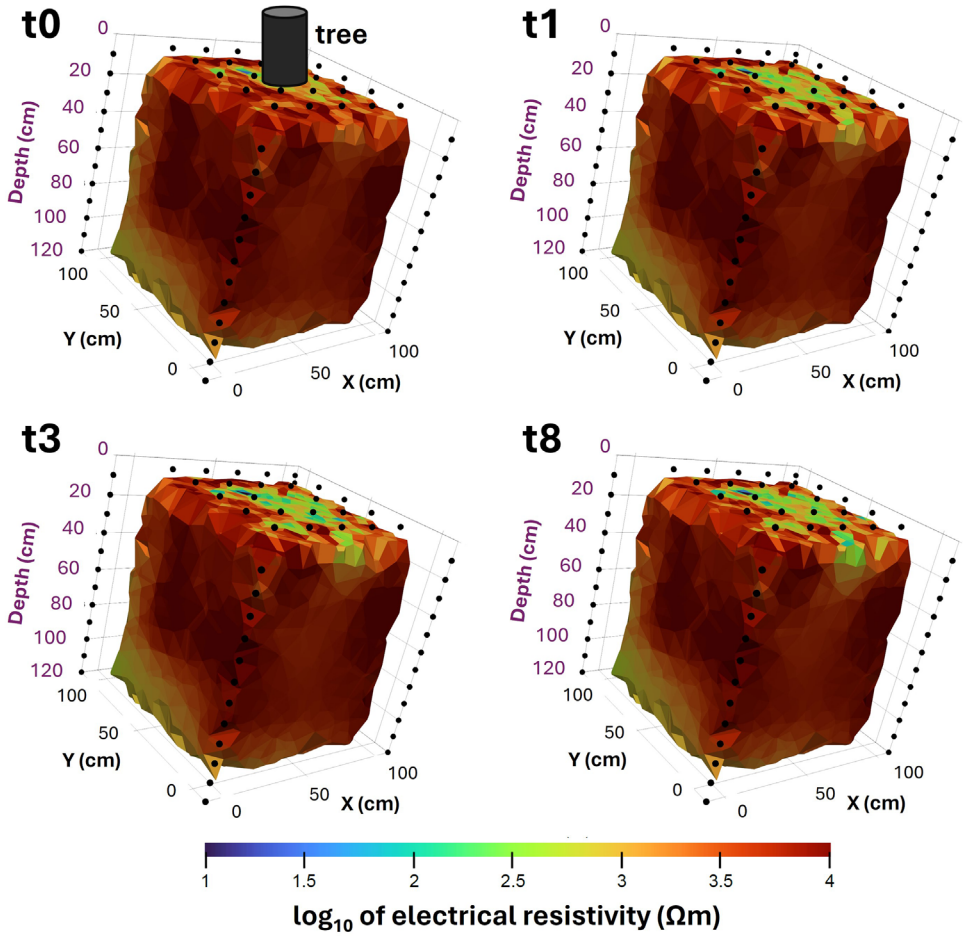

FIGURE 5 Logarithmic values of the electrical resistivity for four different surveys (t0, t1, t3, and t8). Origin of the *X* and *Y* axes differs from those reported in Figure 4, whereas the location of the tree trunk is shown only for t0. Black dots indicate the location of the electrodes.

expansion) and t7 vs. t0 (Figure 7a). The analysis of resistivity variations for the 0–15 cm, 15–30 cm, and 30–45 cm depths showed that very marked changes in resistivity (between −50% and −100%) occurred mostly at the shallowest layer (0–15 cm) (Figure 7b). Variations more extreme than −50% were also detected at the 15–30 cm depth, particularly in the late stages of the experiment (from t5 vs. t0 up to t8 vs. t0) (Figure 7c). On the contrary, at the 30–45 cm depth, the observed resistivity variations were generally less marked (mostly between 0% and −40%) than at the shallower depths (Figure 7d).

By means of the analysis of the relation between depth and frequency of mesh elements in each resistivity variation class, we observed that stemflow infiltration was already evident in t1 vs. t0 in the shallow soil layers (between 0 and 45 cm, Figure 8). In the later stages of the experiment, the wetting front determined an increase in the frequency of mesh elements in all resistivity variation classes, especially at 15–30 cm and 30–45 cm depths. Resistivity variations comprised between −10% and −20% were also found below 60-cm depth during all geophysical surveys, but more marked changes (variations between −20% and −30%) were detected starting from t4 vs. t0 (not shown) up to t8 vs. t0 (Figure 8). Note that the volume that appears to be invaded on the basis of the ERT results is fully compatible with the applied total water volume (26 L) considering the expected soil porosity and considering that, of course, the soil is not fully saturated by the applied water.

3.3 | Estimation of stemflow infiltration area using different approaches

Based on K_{sat} measurements taken close to the beech tree, the estimated I_t varied between a minimum of 0.01 m^2 and a maximum of 0.32 m^2, with an average equal to 0.02 m^2 (n = 8). These values of I_t were much smaller than the stemflow infiltration areas obtained by the analysis of resistivity variations. Indeed, the surface pattern (upper 2 cm of the mesh) of resistivity variation data (only values <−10% were considered) yielded estimations of stemflow infiltration area varying between 0.54 m^2 (t7 vs. t0) and 0.70 m^2 (t4 vs. t0), with an

15391663, 2025, 1, Downloaded from https://acsess.onlinelibrary.wiley.com/doi/10.1002/vzj2.20397 by University Of Padova Center Di, Wiley Online Library on [07/02/2025]. See the Terms and Conditions (https://onlinelibrary.wiley.com/terms-and-conditions) on Wiley Online Library for rules of use; OA articles are governed by the applicable Creative Commons License

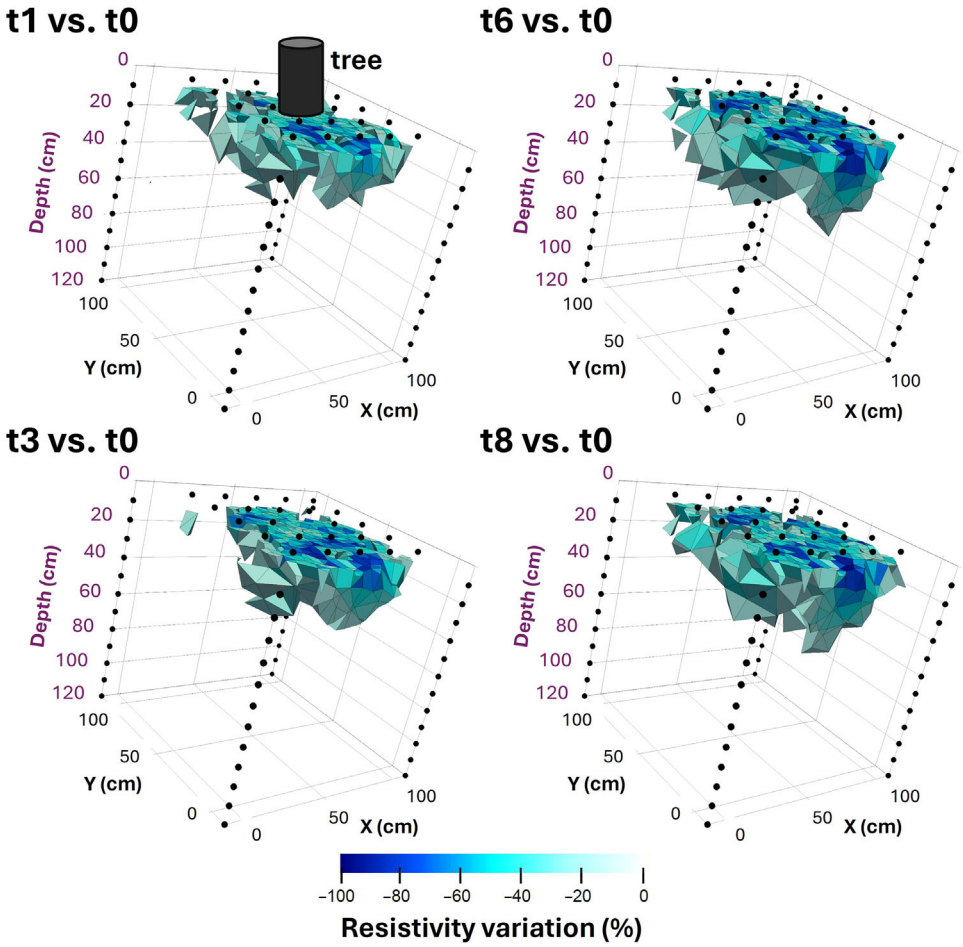

FIGURE 6 Electrical resistivity variations compared to the t0 model. Only negative variations (<−20%) are reported in the figure. Origin of the *X* and *Y* axes differs from those reported in Figure 4, whereas the location of the tree trunk is shown only for t1 vs. t0. Black dots indicate the location of the electrodes.

average of 0.64 m^2. At the end of the stemflow simulation corresponding to t5, stemflow infiltration area was 0.64 m^2. The lower stemflow infiltration area for t7 vs. t0 was expected considering the slightly lower frequencies of negative resistivity variations observed for t7 vs. t0 compared to other geophysical surveys (Figure 7).

Although in this case the isotopic tracer presents certain sampling limitations that are described in Section 2.5.3, the spatial interpolations of the fraction of labeled water (accounting for the uncertainty in the fraction computation) at 0–15 cm yielded areas varying between 0.47 m^2 (Figure 9a) and 0.55 m^2 (Figure 9b), when considering fractions of labeled water >0%. For fractions of labeled water >5%, stemflow infiltration areas were 0.39 m^2 (Figure 9a) and 0.40 m^2 (Figure 9b). These interpolated areas were lower than the values of stemflow infiltration area estimated by resistivity variations (except for t7 vs. t0 which yielded a value very close to the estimates based on the isotopic tracer), but much larger (and probably more reliable) than the indirect I_t estimates. We attribute the variability in the estimations based on the fraction of labeled water to the power, number of neighbors and sector type used in the inverse distance weighting. Note that values of stemflow infiltration area of 0.55 m^2 were basically equal to the total extension of the interpolated area (Figure 9b); this confirms our sampling limitation and that we should have collected more soil samples at greater distances from the tree trunk.

4 | DISCUSSION

4.1 | Advantages and limitations for the application of stable isotopes of hydrogen and oxygen in stemflow experiments

In recent years, δ^2H and $\delta^{18}O$ have been widely applied to study the water fluxes in soil–plant–atmosphere continuum, and particularly to determine plant water uptake (e.g., Orlowski et al., 2023; Penna et al., 2018). However, the application of the isotopic tracers in stemflow experiments is very

15391663, 2025, 1, Downloaded from https://acsess.onlinelibrary.wiley.com/doi/10.1002/vzj2.20397 by University Of Padova Center Di, Wiley Online Library on [07/02/2025]. See the Terms and Conditions (https://onlinelibrary.wiley.com/terms-and-conditions) on Wiley Online Library for rules of use; OA articles are governed by the applicable Creative Commons License

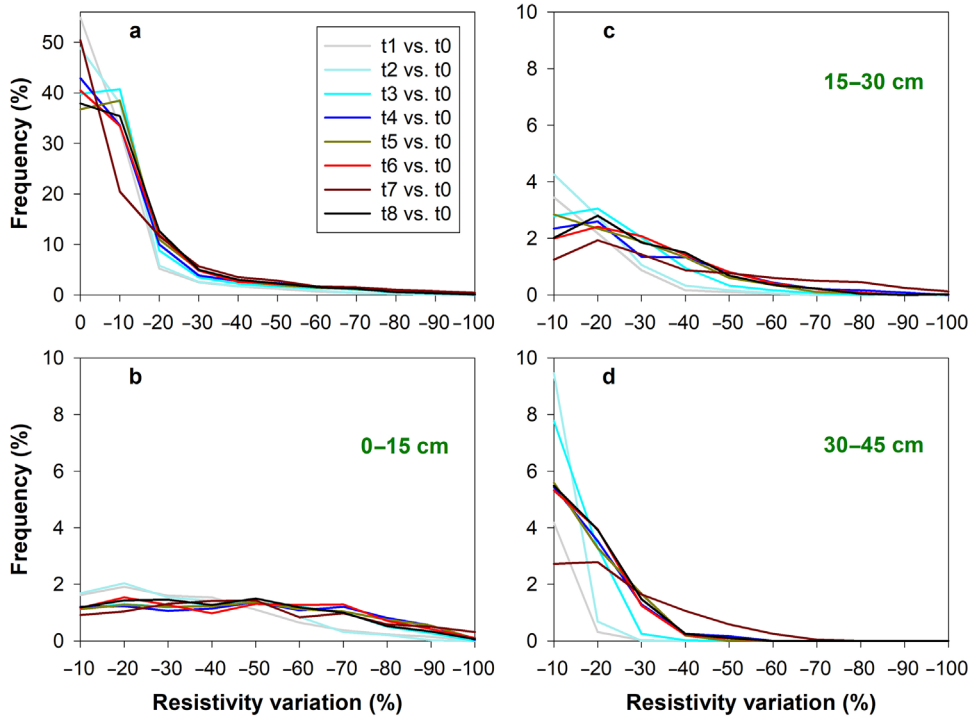

FIGURE 7 Frequency of mesh elements in each resistivity variation class, from t1 vs. t0 up to t8 vs. t0, considering all depths (a), 0–15 cm (b), 15–30 cm (c), and 30–45 cm (d) depths. In the *X* axis, class 0 indicates variations that are positive or equal to zero (this class is not shown in panels b, c, and d), whereas the other displayed values represent the most negative variation in the specific class (e.g., −10 indicates the class with variations comprised between 0% and −10%).

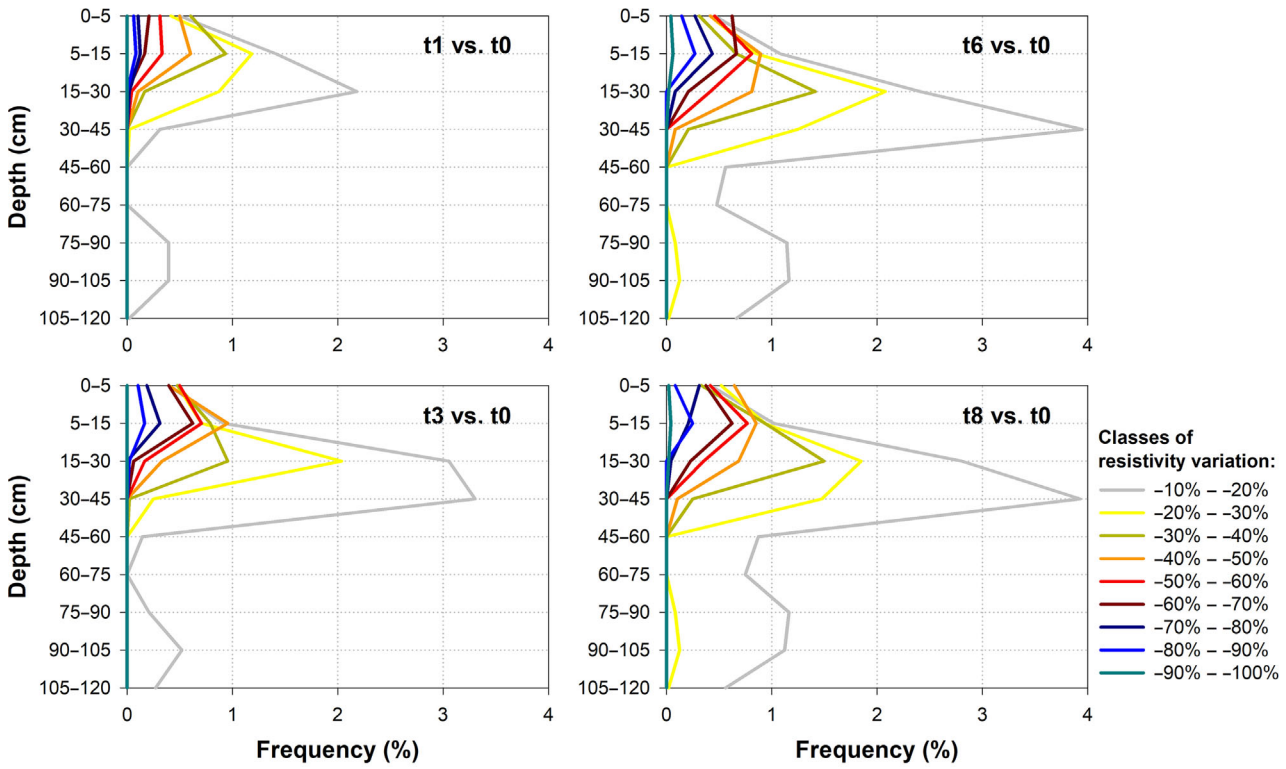

FIGURE 8 Relation between depth and frequency of mesh elements in each resistivity variation class. For a better focus on classes with marked changes and likely less affected by artifacts, classes with resistivity variations ≥0% and between 0% and −10% are not shown.

15391663, 2025, 1, Downloaded from https://acsess.onlinelibrary.wiley.com/doi/10.1002/vzj2.20397 by University Of Padova Center Di, Wiley Online Library on [07/02/2025]. See the Terms and Conditions (https://onlinelibrary.wiley.com/terms-and-conditions) on Wiley Online Library for rules of use; OA articles are governed by the applicable Creative Commons License

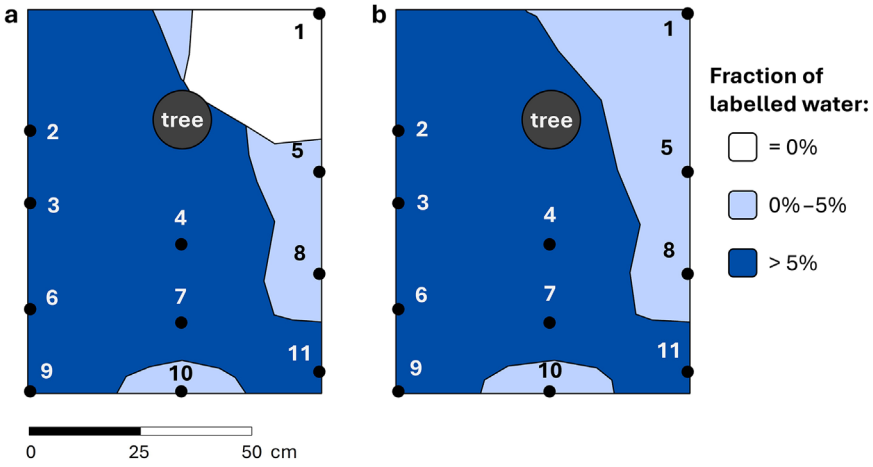

FIGURE 9 Examples of reclassified interpolated fractions of labeled water using different parameter values in the inverse distance weighting. The moving window was 30 cm in both maps, whereas power was 5.8 (a) and 7.2 (b). Root mean square error (RMSE) was 16.8% (a) and 17.1% (b). Black dots and the numbers above indicate the location of the sampling sites for soil water.

rare (Pinos et al., 2023; Van Stan & Allen, 2020). Therefore, our study is the first exploiting isotopically labeled water to trace stemflow infiltration and to attempt at a first estimate of stemflow infiltration area. Compared to Pinos et al. (2023), our setup was much simpler and involved much less excavation at the tree surroundings, and we used water that was much more depleted in heavy isotopes (more negative). Relying only on 11 locations and three depths represents a limitation of our study and prevented us from the investigation of the double-funneling effect along the root system and of the preferential flow. However, our results clearly showed that stemflow infiltration mainly occurred along the maximum slope gradient and involved mostly the upper 30 cm of soil (Figure 4), which was confirmed by the results of the geophysical surveys (Figures 6 and 8). This sampling limitation influenced the estimation of the stemflow infiltration area, which was smaller (up to 0.55 m^2, Figure 9) than the one based on electrical resistivity variations (average of 0.64 m^2). Despite this limitation, our approach for data analysis, that is, based on the fraction of labeled water and accounting for uncertainty (Genereux, 1998), seems sound and enabled us to easily rule out the sampling locations which had a negligible signal of labeled water (Figure 4b). Furthermore, spatial interpolation followed by a reclassification of the areas with a certain fraction of labeled water could be employed successfully for the estimation of stemflow infiltration area based on the isotopic tracer, if the samplings can capture effectively the stemflow infiltration area. In this sense, future studies relying on multiple methods to study stemflow infiltration could exploit the field evidence gained by dye tracers or a rapid preliminary analysis of ERT data, to inform and design the sampling collection of soil samples for the isotopic analysis.

Finally, in our study, we did not observe specific issues related to isotopic fractionation (due to enhanced evaporation) in the soil—probably because the stemflow experiment lasted about 24 h—and to soil water extraction by cryogenic vacuum distillation (Amin et al., 2021; Orlowski et al., 2016, 2018). Indeed, our soil water samples plotted between the labeled water and the pre-experiment soil water and they were close to the LMWL, with a little deviation that was due to the deviation of the pre-experiment soil water from the LMWL and the rain water collected in the previous month (Figure 3). Nonetheless, future studies should consider the sensitivity of the results to isotopic fractionation in the soil water (due to evaporation and/or artifacts related to the water extraction technique), particularly for stemflow experiments lasting multiple days or weeks. In addition, it may be worth to investigate whether a particularly high electrical conductivity of the labeled water (due to the mixing with salt) can pose problems during the soil water extraction and isotopic analysis, similarly to the isotope effect caused by high cation exchange capacity in mineral water systems (Oerter et al., 2014). In our case, the labeled water had an electrical conductivity of 1072 µS/cm, but we did not detect specific issues during the soil water extraction by cryogenic vacuum distillation and isotopic analysis by laser spectroscopy.

4.2 | Advantages and limitations for the application of geophysical approaches in stemflow experiments

The use of minimally-invasive (geophysical) methods has one key advantage over all other subsoil investigation methods, namely its capability of producing extensive (often 3D) reconstructions of a portion of the medium of interest with high resolution (Cassiani et al., 2015; Di Prima et al., 2022; Guo et al., 2020), thus avoiding for instance the inevitable spatial aliasing (Shannon, 1949) induced by interpolating sparse point measurements. Aliasing produces smoother and more extensive anomalies than the sampled data should actually represent. Therefore, geophysical images are much more representative, for example, of the processes taking place such as in this case study, when repeated (time-lapse) measurements are made (Cassiani et al., 2009; Pavoni et al., 2023). In this study, we showed the usefulness of time-lapse ERT

15391663, 2025, 1, Downloaded from https://acsess.onlinelibrary.wiley.com/doi/10.1002/vzj2.20397 by University Of Padova Center Di, Wiley Online Library on [07/02/2025]. See the Terms and Conditions (https://onlinelibrary.wiley.com/terms-and-conditions) on Wiley Online Library for rules of use; OA articles are governed by the applicable Creative Commons License

surveys to successfully trace stemflow infiltration, particularly under a condition of poor contact between the soil and the electrodes. As expected, results based on time-lapse ERT surveys allowed for a better and minimally invasive inspection and analysis of the wetting front (with little effort we reached higher depths and covered a larger volume) compared to the isotopic-based approach. Our results showed that the wetting front expanded mainly downward along the maximum slope gradient and stayed mainly in the upper 30–45 cm of the soil (Figure 8).

The reconstructed 3D mesh of the resistivity variations also allowed an estimation of stemflow infiltration area, which was slightly larger than the one obtained by the isotopic tracer and much larger than the I_t values (range: 0.01–0.32 m^2). Our estimates of the stemflow infiltration area (average of 0.64 m^2 based on resistivity variations) were much larger than the values obtained by previous studies using dye tracers (e.g., 0.245 m^2 in Schwärzel et al. (2012), between 0.0035 and 0.0951 m^2 in Llorens et al. (2022), 0.14 m^2 in Pinos et al. [2023]), and such results were unexpected when we designed the stemflow experiment. On the contrary, our minimum (0.01 m^2) and average I_t (0.02 m^2) were similar to those estimated by Llorens et al. (2022), which varied between 0.003 and 0.04 m^2 based on the infiltrometer approach for K_{sat}.

Our large estimates of stemflow infiltration area based on resistivity variations (and the isotopic-based approach) may be due to the presence of a litter layer that repels water (Iovino et al., 2018; Rye & Smettem, 2017), to soil hydrophobicity under dry conditions, which decreases infiltration rates (Van Stan & Allen, 2020), and to the high slope (27.5°), which determined some overland flow moving downward and a marked lateral distribution of the stemflow. We do not exclude that our setup, with a tube for stemflow simulation placed about 20 cm above the ground, may have generated a too-uniform flow of water compared to stemflow under natural conditions and may be responsible for the large stemflow infiltration areas. Resistivity variations detected along the root surfaces can also cause an overestimation of the volume and area of stemflow infiltration because, without knowing the exact location, distribution, and size of the roots (as in our case), the estimations comprise the root volume and area. Such challenge in the discrimination of roots and soil particles underscores the need for improved ERT data acquisition methods and enhanced processing techniques to address the limitations in resistivity resolution and signal clarity. Similarly to Pinos et al. (2023), we think that our result should be considered with caution because it corresponds to a specific amount (26 L) and intensity (6.6 L/h), specific soil properties, and antecedent moisture conditions (Figure S1). Note also that to enhance the signal of the labeled water in the soil and to better detect the changes in both the isotopic tracer and in resistivity, we carried out the experiment during dry conditions, and we added salt to the water used for the stemflow simulation.

Furthermore, we need to consider that geophysical measurements collect physical information on parameters that correlate but sometimes weakly with the state variable of interest. In this case, ERT produces images of electrical resistivity that correlates, but with some caution, with soil water content: a proper control of water salinity is also necessary, as salinity also changes the electrical conductivity of the porous medium, by changing the conductivity of the pore water. Considering that our stemflow experiment is related to specific conditions (setup, soil properties, and hydrometeorological conditions), future research based on time-lapse ERT should aim at collecting data for a longer period (e.g., it would be interesting to observe the effects of new stemflow with low electrical conductivity on the old wetting front), at estimating stemflow infiltration area for various stemflow amounts and intensities (similarly to the experimental design in Llorens et al. [2022]) and under different antecedent moisture conditions, and verifying the sensitivity of the results to water salinity and artifacts. Our study also calls for new comparisons between the isotopic-based and the ERT-based approaches to provide further recommendations for successful and less invasive applications of the two approaches in stemflow experiments. The results of isotopic-based and the ERT-based approaches should be validated using other methods as well. For instance, besides the application of dye tracers, the measurements of soil hydraulic properties, soil texture, organic carbon content, and pH at different distances from the tree stems can provide further evidence on stemflow infiltration areas and spatial patterns (Metzger et al., 2021).

5 | CONCLUSION

In this study, we show the results of the first study combining isotopic tracers (^2H and ^{18}O) and time-lapse ERT to trace stemflow infiltration. Our findings suggest that simulating stemflow with an isotopic composition very different from that of soil water can be effective for the identification of the main pathways of stemflow in the soil. Specifically, the estimation of the fraction of labeled water based on a simple two-component mixing model accounting for uncertainty could be applied to easily rule out sites with a negligible signal of stemflow. Furthermore, spatial interpolation of the fraction of labeled water could be used to estimate stemflow infiltration area, if the sampling design captured well the extension of stemflow infiltration. This means that future studies based on isotopic tracers need to consider methods providing a direct field evidence of stemflow infiltration (e.g., dye tracers) or a quick inspection of raw data (e.g., ERT) to inform and properly choose the sampling design for the soil sample collection. However, due to the destructive soil samplings, an

15391663, 2025, 1, Downloaded from https://acsess.onlinelibrary.wiley.com/doi/10.1002/vzj2.20397 by University Of Padova Center Di, Wiley Online Library on [07/02/2025]. See the Terms and Conditions (https://onlinelibrary.wiley.com/terms-and-conditions) on Wiley Online Library for rules of use; OA articles are governed by the applicable Creative Commons License

isotopic-based approach is much more invasive and less repeatable than ERT surveys.

The analysis of electrical resistivity variations enabled to evaluate the temporal dynamics of stemflow infiltration and to estimate an average stemflow infiltration area of 0.64 m^2, which was much larger than values found by previous literature studies based on dye tracers. Our high estimate may be due to the repellency of the litter layer, soil hydrophobicity under dry conditions, and the steepness of the site, as well as to a too-uniform simulated stemflow and uncertainty in the resistivity variations along the root surfaces. We acknowledge that our stemflow experiment also had a specific setup (e.g., stemflow amount and intensity) and was carried out under specific antecedent moisture conditions and soil properties. Therefore, we call for new research, based on both methodologies, to trace stemflow infiltration under different conditions and to evaluate the advantages and drawbacks of the two approaches.

AUTHOR CONTRIBUTIONS

Giulia Zuecco: Conceptualization; data curation; formal analysis; investigation; methodology; visualization; writing—original draft; writing—review and editing. **Chiara Marchina**: Data curation; investigation; methodology; visualization; writing—original draft; writing—review and editing. **Matteo Censini**: Data curation; formal analysis; investigation; methodology; visualization; writing—original draft; writing—review and editing. **Diego Todini-Zicavo**: Investigation; writing—review and editing. **Giorgio Cassiani**: Funding acquisition; supervision; writing—review and editing. **Marco Borga**: Funding acquisition; project administration; supervision; writing—review and editing.

ACKNOWLEDGMENTS

Samplings, laboratory activities, and data analysis carried out for this study were supported by the Italian MIUR Project (PRIN 2017) "WATer mixing in the critical ZONe: observations and predictions under environmental changes-WATZON" (code: 2017SL7ABC, national coordinator: Marco Borga). The authors would like to thank Stefano Brighenti (Free University of Bozen-Bolzano, Italy) for his supervision during the soil water extraction by cryogenic vacuum distillation, and Enrico Marin (University of Padova, Italy) for his assistance with field measurements.

CONFLICT OF INTEREST STATEMENT

The authors declare no conflict of interest.

ORCID

G. Zuecco https://orcid.org/0000-0002-2125-0717
C. Marchina https://orcid.org/0000-0002-8496-635X
G. Cassiani https://orcid.org/0000-0002-9060-5606
M. Borga https://orcid.org/0000-0003-3435-2779

REFERENCES

Amin, A., Zuecco, G., Marchina, C., Engel, M., Penna, D., McDonnell, J. J., & Borga, M. (2021). No evidence of isotopic fractionation in olive trees (*Olea europaea*): A stable isotope tracing experiment. *Hydrological Sciences Journal*, *66*(16), 2415–2430. https://doi.org/10.1080/02626667.2021.1987440

Bagarello, V., Castellini, M., Di Prima, S., Giordano, G., & Iovino, M. (2013). Testing a simplified approach to determine field saturated soil hydraulic conductivity. *Procedia Environmental Sciences*, *19*, 599–608. https://doi.org/10.1016/j.proenv.2013.06.068

Bagarello, V., Di Prima, S., Iovino, M., & Provenzano, G. (2014). Estimating field-saturated soil hydraulic conductivity by a simplified Beerkan infiltration experiment. *Hydrological Processes*, *28*, 1095–1103. https://doi.org/10.1002/hyp.9649

Bialkowski, R., & Buttle, J. M. (2015). Stemflow and throughfall contributions to soil water recharge under trees with differing branch architectures. *Hydrological Processes*, *29*, 4068–4082. https://doi.org/10.1002/hyp.10463

Binley, A. (2015). Tools and techniques: Electrical methods. In G. Schubert (Ed.), *Treatise on geophysics* (2nd ed., Vol. 11, pp. 233–259). Elsevier. https://doi.org/10.1016/B978-0-444-53802-4.00192-5

Binley, A., & Kemna, A. (2005). DC resistivity and induced polarization methods. In Y. Rubin & S. S. Hubbard (Eds.), *Hydrogeophysics. Water science and technology library* (Vol. 50, pp. 129–156). Springer. https://doi.org/10.1007/1-4020-3102-5_5

Blanchy, G., Saneiyan, S., Boyd, J., McLachlan, P., & Binley, A. (2020). ResIPy, an intuitive open source software for complex geoelectrical inversion/modeling. *Computers & Geosciences*, *137*, 104423. https://doi.org/10.1016/j.cageo.2020.104423

Brighenti, S., Obojes, N., Bertoldi, G., Zuecco, G., Censini, M., Cassiani, G., Penna, D., & Comiti, F. (2024). Snowmelt and subsurface heterogeneity control tree water sources in a subalpine forest. *Ecohydrology*, *17*(7), e2695. https://doi.org/10.1002/eco.2695

Bouten, W., Heimovaara, T. J., & Tiktak, A. (1992). Spatial patterns of throughfall and soil water dynamics in a Douglas fir stand. *Water Resources Research*, *28*(12), 3227–3233. https://doi.org/10.1029/92WR01764

Carlyle-Moses, D. E., Iida, S. I., Germer, S., Llorens, P., Michalzik, B., Nanko, K., Tanaka, T., Tischer, A., & Levia, D. F. (2020). Commentary: What we know about stemflow's infiltration area. *Frontiers in Forests and Global Change*, *3*, 577247. https://doi.org/10.3389/ffgc.2020.577247

Carlyle-Moses, D. E., Iida, S. I., Germer, S., Llorens, P., Michalzik, B., Nanko, K., Tischer, A., & Levia, D. F. (2018). Expressing stemflow commensurate with its ecohydrological importance. *Advances in Water Resources*, *121*, 472–479. https://doi.org/10.1016/j.advwatres.2018.08.015

Cassiani, G., Boaga, J., Rossi, M., Putti, M., Fadda, G., Majone, B., & Bellin, A. (2016). Soil-plant interaction monitoring: Small scale example of an apple orchard in Trentino, North-Eastern Italy. *Science of the Total Environment*, *543*(Part B), 851–861. https://doi.org/10.1016/j.scitotenv.2015.03.113

Cassiani, G., Boaga, J., Vanella, D., Perri, M. T., & Consoli, S. (2015). Monitoring and modelling of soil–plant interactions: The joint use of ERT, sap flow and eddy covariance data to characterize the volume of an orange tree root zone. *Hydrology and Earth System Sciences*, *19*, 2213–2225. https://doi.org/10.5194/hess-19-2213-2015

Cassiani, G., Godio, A., Stocco, S., Villa, A., Deiana, R., Frattini, P., & Rossi, M. (2009). Monitoring the hydrologic behavior of a mountain

15391663, 2025, 1, Downloaded from https://acsess.onlinelibrary.wiley.com/doi/10.1002/vzj2.20397 by University Of Padova Center Di, Wiley Online Library on [07/02/2025]. See the Terms and Conditions (https://onlinelibrary.wiley.com/terms-and-conditions) on Wiley Online Library for rules of use; OA articles are governed by the applicable Creative Commons License

slope via time-lapse electrical resistivity tomography. *Near Surface Geophysics*, *7*, 475–486. https://doi.org/10.3997/1873-0604.2009013

Dick, J., Tetzlaff, D., Bradford, J., & Soulsby, C. (2018). Using repeat electrical resistivity surveys to assess heterogeneity in soil moisture dynamics under contrasting vegetation types. *Journal of Hydrology*, *559*, 684–697. https://doi.org/10.1016/j.jhydrol.2018.02.062

Di Prima, S., Giannini, V., Ribeiro Roder, L., Giadrossich, F., Lassabatere, L., Stewart, R. D., Abou Najm, M. R., Longo, V., Campus, S., Winiarski, T., Angulo-Jaramillo, R., del Campo, A., Capello, G., Bidoccu, M., Roggero, P. P., & Pirastru, M. (2022). Coupling time-lapse ground penetrating radar surveys and infiltration experiments to characterize two types of non-uniform flow. *Science of the Total Environment*, *806*, 150410. https://doi.org/10.1016/j.scitotenv.2021.150410

Genereux, D. (1998). Quantifying uncertainty in tracer-based hydrograph separations. *Water Resources Research*, *34*(4), 915–919. https://doi.org/10.1029/98WR00010

Germer, S., Werther, L., & Elsenbeer, H. (2010). Have we underestimated stemflow? Lessons from an open tropical rainforest. *Journal of Hydrology*, *395*, 169–179. https://doi.org/10.1016/j.jhydrol.2010.10.022

Gonzalez-Ollauri, A., Stokes, A., & Mickovski, S. B. (2020). A novel framework to study the effect of tree architectural traits on stemflow yield and its consequences for soil-water dynamics. *Journal of Hydrology*, *582*, 124448. https://doi.org/10.1016/j.jhydrol.2019.124448

Guerrieri, R., Vanguelova, E. I., Michalski, G., Heaton, T. H. E., & Mencuccini, M. (2015). Isotopic evidence for the occurrence of biological nitrification and nitrogen deposition processing in forest canopies. *Global Change Biology*, *21*, 4613–4626. https://doi.org/10.1111/gcb.13018

Guo, L., Mount, G. J., Hudson, S., Lin, H., & Levia, D. (2020). Pairing geophysical techniques improves understanding of the near-surface Critical Zone: Visualization of preferential routing of stemflow along coarse roots. *Geoderma*, *357*, 113953. https://doi.org/10.1016/j.geoderma.2019.113953

Herwitz, S. R. (1986). Infiltration-excess caused by stemflow in a cyclone-prone tropical rainforest. *Earth Surface Processes and Landforms*, *11*(4), 401–412. https://doi.org/10.1002/esp.3290110406

Iovino, M., Pekárová, P., Hallett, P. D., Pekár, J., Lichner, L., Mataix-Solera, J., Alagna, V., Walsh, R., Raffan, A., Schacht, K., & Rodný, M. (2018). Extent and persistence of soil water repellency induced by pines in different geographic regions. *Journal of Hydrology and Hydromechanics*, *66*, 360–368. https://doi.org/10.2478/johh-2018-0024

Koeniger, P., Marshall, J. D., Link, T., & Mulch, A. (2011). An inexpensive, fast, and reliable method for vacuum extraction of soil and plant water for stable isotope analyses by mass spectrometry. *Rapid Communications in Mass Spectrometry*, *25*(20), 3041–3048. https://doi.org/10.1002/rcm.5198

Levia, D. F., & Frost, E. E. (2006). Variability of throughfall volume and solute inputs in wooded ecosystems. *Progress in Physical Geography*, *30*(5), 605–632. https://doi.org/10.1177/0309133306071145

Liang, W.-L., Kosugi, K., & Mizuyama, T. (2011). Soil water dynamics around a tree on a hillslope with or without rainwater supplied by stemflow. *Water Resources Research*, *47*, W02541. https://doi.org/10.1029/2010WR009856

Llorens, P., Latron, J., Carlyle-Moses, D. E., Näthe, K., Chang, J. L., Nanko, K., Iida, S., & Levia, D. F. (2022). Stemflow infiltration areas into forest soils around American beech (*Fagus grandifolia* Ehrh.) trees. *Ecohydrology*, *15*(2), e2369. https://doi.org/10.1002/eco.2369

Marchina, C., Zuecco, G., Chiogna, G., Bianchini, G., Carturan, L., Comiti, F., Engel, M., Natali, C., Borga, M., & Penna, D. (2020). Alternative methods to determine the δ^2H-δ^{18}O relationship: An application to different water types. *Journal of Hydrology*, *587*, 124951. https://doi.org/10.1016/j.jhydrol.2020.124951

Mary, B., Peruzzo, L., Boaga, J., Schmutz, M., Wu, Y., Hubbard, S. S., & Cassiani, G. (2018). Small-scale characterization of vine plant root water uptake via 3-D electrical resistivity tomography and mise-à-la-masse method. *Hydrology and Earth System Sciences*, *22*, 5427–5444. https://doi.org/10.5194/hess-22-5427-2018

Metzger, J. C., Filipzik, J., Michalzik, B., & Hildebrandt, A. (2021). Stemflow infiltration hotspots create soil microsites near tree stems in an unmanaged mixed beech forest. *Frontiers in Forests and Global Change*, *4*, 701293. https://doi.org/10.3389/ffgc.2021.701293

Metzger, J. C., Wutzler, T., Dalla Valle, N., Filipzik, J., Grauer, C., Lehmann, R., Roggenbuck, M., Schelhorn, D., Weckmüller, J., Küsel, K., Totsche, K. U., Trumbore, S., & Hildebrandt, A. (2017). Vegetation impacts soil water content patterns by shaping canopy water fluxes and soil properties. *Hydrological Processes*, *31*(22), 3783–3795. https://doi.org/10.1002/hyp.11274

Molina, A. J., Llorens, P., Garcia-Estringana, P., Moreno de las Heras, M., Cayuela, C., Gallart, F., & Latron, J. (2019). Contributions of throughfall, forest and soil characteristics to near-surface soil water-content variability at the plot scale in a mountainous Mediterranean area. *Science of the Total Environment*, *647*, 1421–1432. https://doi.org/10.1016/j.scitotenv.2018.08.020

Oerter, E., Finstad, K., Schaefer, J., Goldsmith, G. R., Dawson, T., & Amundson, R. (2014). Oxygen isotope fractionation effects in soil water via interaction with cations (Mg, Ca, K, Na) adsorbed to phyllosilicate clay minerals. *Journal of Hydrology*, *515*, 1–9. https://doi.org/10.1016/j.jhydrol.2014.04.029

Orlowski, N., Breuer, L., Angeli, N., Boeckx, P., Brumbt, C., Cook, C. S., Dubbert, M., Dyckmans, J., Gallagher, B., Gralher, B., Herbstritt, B., Hervé-Fernández, P., Hissler, C., Koeniger, P., Legout, A., Macdonald, C. J., Oyarzún, C., Redelstein, R., Seidler, C., … McDonnell, J. J. (2018). Inter-laboratory comparison of cryogenic water extraction systems for stable isotope analysis of soil water. *Hydrology and Earth System Sciences*, *22*, 3619–3637. https://doi.org/10.5194/hess-22-3619-2018

Orlowski, N., Pratt, D. L., & McDonnell, J. J. (2016). Intercomparison of soil pore water extraction methods for stable isotope analysis. *Hydrological Processes*, *30*, 3434–3449. https://doi.org/10.1002/hyp.10870

Orlowski, N., Rinderer, M., Dubbert, M., Ceperley, N., Hrachowitz, M., Gessler, A., Rothfuss, Y., Sprenger, M., Heidbüchel, I., Kübert, A., Beyer, M., Zuecco, G., & McCarter, C. (2023). Challenges in studying water fluxes within the soil-plant-atmosphere continuum: A tracer-based perspective on pathways to progress. *Science of the Total Environment*, *881*, 163510. https://doi.org/10.1016/j.scitotenv.2023.163510

Oyarzún, C. E., Godoy, R., De Schrijver, A., Staelens, J., & Lust, N. (2004). Water chemistry and nutrient budgets in an undisturbed evergreen rainforest of southern Chile. *Biogeochemistry*, *71*, 107–123. https://doi.org/10.1007/s10533-004-4107-x

15391663, 2025, 1, Downloaded from https://acsess.onlinelibrary.wiley.com/doi/10.1002/vzj2.20397 by University Of Padova Center Di, Wiley Online Library on [07/02/2025]. See the Terms and Conditions (https://onlinelibrary.wiley.com/terms-and-conditions) on Wiley Online Library for rules of use; OA articles are governed by the applicable Creative Commons License

Pavoni, M., Boaga, J., Carrera, A., Zuecco, G., Carturan, L., & Zumiani, M. (2023). Brief communication: Mountain permafrost acts as an aquitard during an infiltration experiment monitored with electrical resistivity tomography time-lapse measurements. *The Cryosphere*, *17*, 1601–1607. https://doi.org/10.5194/tc-17-1601-2023

Penna, D., Hopp, L., Scandellari, F., Allen, S. T., Benettin, P., Beyer, M., Geris, J., Klaus, J., Marshall, J. D., Schwendenmann, L., Volkmann, T. H. M., von Freyberg, J., Amin, A., Ceperley, N., Engel, M., Frentress, J., Giambastiani, Y., McDonnell, J. J., Zuecco, G., … Kirchner, J. W. (2018). Ideas and perspectives: Tracing terrestrial ecosystem water fluxes using hydrogen and oxygen stable isotopes—Challenges and opportunities from an interdisciplinary perspective. *Biogeosciences*, *15*, 6399–6415. https://doi.org/10.5194/bg-15-6399-2018

Penna, D., van Meerveld, H. J., Oliviero, O., Zuecco, G., Assendelft, R. S., Dalla Fontana, G., & Borga, M. (2015). Seasonal changes in runoff generation in a small forested mountain catchment. *Hydrological Processes*, *29*, 2027–2042. https://doi.org/10.1002/hyp.10347

Pinder, G. F., & Jones, J. F. (1969). Determination of groundwater component of peak discharge from chemistry of total runoff. *Water Resources Research*, *5*(2), 438–445. https://doi.org/10.1029/WR005i002p00438

Pinos, J., Flury, M., Latron, J., & Llorens, P. (2023). Routing stemflow water through the soil via preferential flow: A dual-labelling approach with artificial tracers. *Hydrology and Earth System Sciences*, *27*, 2865–2881. https://doi.org/10.5194/hess-27-2865-2023

Pinos, J., Latron, J., Levia, D. F., & Llorens, P. (2021). Drivers of the circumferential variation of stemflow inputs on the boles of *Pinus sylvestris* L. (*Scots pine*). *Ecohydrology*, *14*, e2348. https://doi.org/10.1002/eco.2348

Preti, F., Guastini, E., Penna, D., Dani, A., Cassiani, G., Boaga, J., Deiana, R., Romano, N., Nasta, P., Palladino, M., Errico, A., Giambastiani, Y., Trucchi, P., & Tarolli, P. (2018). Conceptualization of water flow pathways in agricultural terraced landscapes. *Land Degradation & Development*, *29*(3), 651–662. https://doi.org/10.1002/ldr.2764

Reynolds, E. R. C., & Henderson, C. S. (1967). Rainfall interception by beech, larch and Norway spruce. *Forestry: An International Journal of Forest Research*, *40*(2), 165–184. https://doi.org/10.1093/forestry/40.2.165

Reynolds, W. D., Elrick, D. E., & Youngs, E. G. (2002). 3.4.3.2 Ring or cylinder infiltrometers (vadose zone). In J. H. Dane & G. C. Topp (Eds.), *Methods of soil analysis, part 4, physical methods* (pp. 818–820). Soil Science Society of America. https://doi.org/10.2136/sssabookser5.4.c32

Rye, C. F., & Smettem, K. R. J. (2017). The effect of water repellent soil surface layers on preferential flow and bare soil evaporation. *Geoderma*, *289*, 142–149. https://doi.org/10.1016/j.geoderma.2016.11.032

Schwärzel, K., Ebermann, S., & Schalling, N. (2012). Evidence of double-funneling of beech trees by visualization of flow pathways using dye tracer. *Journal of Hydrology*, *470–471*, 184–192. https://doi.org/10.1016/j.jhydrol.2012.08.048

Shannon, C. E. (1949). Communication in the presence of noise. *Proceedings of the Institute of Radio Engineers*, *37*(1), 10–21. https://doi.org/10.1109/JRPROC.1949.232969

Sklash, M. G., & Farvolden, R. N. (1979). Role of groundwater in storm runoff. *Journal of Hydrology*, *43*(1–4), 45–65. https://doi.org/10.1016/0022-1694(79)90164-1

Spencer, S. A., & van Meerveld, H. J. (2016). Double funnelling in a mature coastal British Columbia forest: Spatial patterns of stemflow after infiltration. *Hydrological Processes*, *30*(22), 4185–4201. https://doi.org/10.1002/hyp.10936

Van Stan, J. T., II, & Allen, S. T. (2020). What we know about stemflow's infiltration area. *Frontiers in Forests and Global Change*, *3*, 61. https://doi.org/10.3389/ffgc.2020.00061

Van Stan, J. T., II, & Pinos, J. (2024). Three fundamental challenges to the advancement of stemflow research and its integration into natural science. *Water*, *16*, 117. https://doi.org/10.3390/w16010117

Xia, C., Zuecco, G., Marchina, C., Penna, D., & Borga, M. (2024). Effects of short-term climate variations on young water fraction in a small pre-Alpine catchment. *Water Resources Research*, *60*, e2023WR036245. https://doi.org/10.1029/2023WR036245

Zimmermann, A., Germer, S., Neill, C., Krusche, A. V., & Elsenbeer, H. (2008). Spatio-temporal patterns of throughfall and solute deposition in an open tropical rain forest. *Journal of Hydrology*, *360*, 87–102. https://doi.org/10.1016/j.jhydrol.2008.07.028

Zuecco, G., Amin, A., Frentress, J., Engel, M., Marchina, C., Anfodillo, T., Borga, M., Carraro, V., Scandellari, F., Tagliavini, M., Zanotelli, D., Comiti, F., & Penna, D. (2022). A comparative study of plant water extraction methods for isotopic analyses: Scholander-type pressure chamber vs. cryogenic vacuum distillation. *Hydrology and Earth System Sciences*, *26*, 3673–3689. https://doi.org/10.5194/hess-26-3673-2022

Zuecco, G., Marchina, C., Gelmini, Y., Amin, A., van Meerveld, H. J., Penna, D., & Borga, M. (2021). Ressi experimental catchment: Eco-hydrological research in the Italian pre-Alps. *Hydrological Processes*, *35*, e14095. https://doi.org/10.1002/hyp.14095

Zuo, F.-L., Li, X.-Y., Yang, X.-F., Ma, Y.-J., Shi, F.-Z., Liao, Q.-W., Li, D.-S., Wang, Y., & Wang, R.-D. (2021). Linking root traits and soil moisture redistribution under *Achnatherum splendens* using electrical resistivity tomography and dye experiments. *Geoderma*, *386*, 114908. https://doi.org/10.1016/j.geoderma.2020.114908

SUPPORTING INFORMATION

Additional supporting information can be found online in the Supporting Information section at the end of this article.

How to cite this article: Zuecco, G., Marchina, C., Censini, M., Todini-Zicavo, D., Cassiani, G., & Borga, M. (2025). A simple experiment to trace stemflow infiltration: Advantages and challenges of using stable isotopes of hydrogen and oxygen and electrical resistivity tomography. *Vadose Zone Journal*, *24*, e20397. https://doi.org/10.1002/vzj2.20397

15391663, 2025, 1, Downloaded from https://acsess.onlinelibrary.wiley.com/doi/10.1002/vzj2.20397 by University Of Padova Center Di, Wiley Online Library on [07/02/2025]. See the Terms and Conditions (https://onlinelibrary.wiley.com/terms-and-conditions) on Wiley Online Library for rules of use; OA articles are governed by the applicable Creative Commons License